FINITE ELEMENT MODELLING OF TOW GEOMETRY IN 3D WOVEN FABRICS

Authors: Y. Mahadik and S.R. Hallett

Advanced Composites Centre for Innovation and Science, Univeristy of Bristol,

University Walk, Bristol, BS8 1TR.

Email: ym1191@bristol.ac.uk

ABSTRACT

A finite element model of a 3D woven angle interlock fabric undergoing compaction based on the multi-element digital chain technique has been developed. The aim of this study was to create a kinematic model to predict the internal architectural features of a 3D woven fabric in a commercial off-the-shelf code. The model geometry was created in MSC. Patran and is run in the explicit finite element software LS-Dyna. A statistical analysis of yarn crimp and resin channel size was carried out on sections from the model at increasing levels of compaction and compared to Resin Transfer Moulded (RTM) manufactured samples of 3D woven fabric with the same weave style. Results show a good correlation between overall mean crimp values in the warp, weft and weaver yarns as well as reasonable accuracy in the frequency distribution of local crimp angles. The trend in resin channel size with respect to increasing levels of compaction was also good but significant discrepancies in the absolute dimensions of a resin channel were present due to limitations in controlling the yarn bundle internal interactions in the model.

INTRODUCTION

Woven fabrics are currently being widely used in composite manufacture leading to a great deal of interest in modelling their behaviour. Both conventional 2D weaves as well as more complex 3D woven fabrics (where layers of yarns are interlaced by through-thickness weaver yarns) exhibit complex internal architectures that make accurate modelling difficult.

The desire to predict the behaviour of woven composite structures has led to the study of many modelling techniques that focus on deriving the overall mechanical properties of a complex woven composite that have been summarised in various papers [1-3].

A widely used method is the 3D mosaic or brick method. This technique splits the fabric structure into small "3D voxel" finite elements. Each element is given the effective combined properties of the fibre orientation, resin content and volume fraction present in that particular section of composite. These discrete homogenous bricks are combined to represent the entire fabric structure [4-6].

This method works well when the overall composite mechanical properties are required. One of the acknowledged disadvantages of the mosaic method is the lack of information on local deformation and the detailed architectural features of the composite [7]. This includes the distortion of local tow geometry such as crimping and twisting of the fabric tows. Local architectural features such as tow crimp and cross-sectional shape can be critical to failure modes and can have a large impact on composite behaviour.

Furthermore, the initial geometry of the fabric used to generate the mesh is often an idealised representation of a real fabric, created in textile generation software. Such packages produce fabric structures that have several limitations including idealised yarn cross sections, yarn spacing, and little modelling of architectural deformations, for example fabric behaviour under compaction. The deformation of fabrics under the influence of forming forces is particularly important and can produce peculiar artefacts in a 3D woven composite geometry.

Several studies have attempted to develop a predictive method that can account for the two major characteristics of yarn deformation under compaction: out of plane crimp and cross section shape changes. Chen and Chou [8] modelled yarns as elastic beams and used beam bending theory to model yarn deformation under compaction. They allowed the shape of the yarn cross section to change under pressure but kept the area constant. Lomov et al. [3,9] employed thorough mechanical characterisation of fabric yarns to develop a predictive model that could take into account yarn bending and compression in an elastic beam model that can be used to generate virtual compression of an FE model. Potluri at al [10] conducted a similar experimental characterisation of a biaxial fabric but also included microscopic analysis to model tow paths and section deformation under various loading regimes. Chen et al [11,12] not only considered yarn crimp and cross-section flattening but also the contact area and forces and nesting between layers of biaxial fabric.

Implementation of 3D finite elements in yarn modelling has been carried out by Potluri et al. [13] and Lin et al. [14]. These models provide more detailed representations of

yarn geometry and spatially varying material properties as well as yarn interactions such as friction and hysteresis. This method has been extended to 3D woven fabrics under compaction by Potluri et al. [15].

Although these studies could produce yarn architectures that represent some of the features of a compacted fabric, they are limited by focussing on very small sections of fabric and still depend on idealised initial tow paths and cross-section shapes that are then subsequently deformed. The complex behaviour of nesting between multiple fabric layers is also neglected and overall deflections are small. More complex weaves in 3D woven fabrics may not exhibit easily quantifiable unit cells and show more significant yarn distortions in heavily compacted states than these idealised structures can account for.

A yarn modelling method that could represent the flexibility of yarn more fully was established by Wang and Sun [16] with the idea of a “digital element” model that was applied to simulate textile processes and to predict the micro geometry of textile fabrics. The model represents a yarn as a chain of pin-connected beams. The pin connection is frictionless and as the individual element length tends to zero approximates the behaviour of a flexible yarn, with contact between yarns is handled by a contact element. A similar method was also proposed by Durville [17].

Miao et al. [18]and Zhou et al. [19, 20] extended this idea by modelling a single yarn as a bundle of digital-element chains. This makes a single digital-element chain analogous to a bundle of fibres within a yarn and gives the “multi-chain” digital element method

the ability to simulate tow cross section deformation as well as the distortion of large yarn assemblies [20].

This study presents a development of the digital chain technique using a commercial off the shelf code and application to predict the internal architecture of an angle interlock fabric under compaction. The study focussed on a statistical analysis of out of plane crimp of the yarns as well as the size and shape of inter-yarn resin channels. The results taken from the finite element model were verified by comparison with experimental results from a previous study [21].

MESHING

A finite element model of a layer-to-layer angle interlock weave 3D woven fabric was created (see Figure 1). Fabric yarns were represented as a bundle of 1D beams. The model was designed to be a kinematic representation of a fabric under compaction, and intended to show the change in crimp during compaction as well as other properties such as nesting of the yarns. The model mesh was created in MSC. Patran and solved in LS-Dyna.

The mesh was designed to be a “loose-weave” which would be tensioned to achieve a final thickness and architecture to match that of the uncompressed weave. It is then compressed in the analysis by rigid plates to simulate the compaction of the fabric in a manufacturing mould.

The critical requirement was a mesh of beam bundles representing yarns that interlace but did not intersect each other. The finite element mesh created in MSC. Patran was based on a repeating cell of the fabric structure. The fabric architecture properties, the warp and weft yarn spacing, tow cross sectional area and the length of the binder repeating unit were measured from the images of the fabric that were used in the sections above.

The unit cell consisted of a single repeating unit of the warp weaver with the cross sections of the perpendicular weft shifted to lie above or below the weaver section. The centre line of a weaver was represented by a cubic curve to create one repeat of the binder path (Figure 2).

This repeating unit was duplicated along its length and then repeated across the fabric in the weft direction in accordance with the weave pattern. This produced a series of points along each weft yarn that can be joined to give a weft yarn centreline that interlaces correctly with the binder. Straight warp centre lines were than inserted in accordance with the weave pattern.

Figure 1 Schematic of layer-to-layer angle interlock fabric.

Figure 2 Schematic of the finite element mesh unit cell and tow beam bundle configuration.

The result of this process was a mesh of one layer of 3D yarns represented by the yarn centrelines, with spacing to allow the insertion of tow bundles around this centreline. This layer could be shifted and duplicated in the thickness direction to create the complete fabric (see
Figure ***3***).

The yarn bundles in the repeating unit were considered to lie in a circular pattern around the tow centre line in the initial mesh with the intention of them taking on their final lenticular shape upon tensioning and compacting. The cross section of each constituent beam element of the bundle was circular. All yarns in both the warp and weft directions were initially meshed using nineteen beams in a concentric pattern around the yarn centreline. This initial cross section shape of the complete bundle was kept constant for the entire length of each yarn. The cross section area of the bundle itself was chosen to match tow cross-sections measured from micrographs of potted samples of the fabric. The average section area from several micrographs were used and applied to every tow in the model.

The ends of the warp weavers, warp and weft yarns were extended away from the interlaced zone in order to allow boundary conditions to be applied far from the area where the fabric was to be compacted. This was chosen to represent the compaction of a small section of a large fabric sample and to minimise possible edge effects. The compaction plates were each meshed as single 4-noded shell elements 2mm thick.

The mesh produced in MSC. Patran was exported as an LS-Dyna keyword file. Boundary conditions, loading, material properties and contact definition were all defined in the Oasys Primer pre-processing software.

Figure 3 Final finite element mesh with sections through interlaced region inset.

MATERIAL PROPERTIES

Initial trials modelled the material of each beam bundle as elastic or elastic-plastic. It was found that using an elastic material made for unstable contacts and erratic movement of elements. Plastic material models were much more stable but showed plastic strain under large displacements which was unrealistic but minimised by the excess yarn lengths. The density, stiffness, Poisson's ratio and plastic yield stress were set to arbitrary values initially and adjusted to minimise model run time rather than to accurately model the yarn properties. The model was created to provide a kinematic representation of the fabric so accurate material properties were not paramount. Sensitivity checks for the stiffness and plastic yield stress were made by running simulations with these properties varied by orders of magnitude. No noticeable change in the final mesh geometry was seen but low plastic yield stresses produced erratic movement of elements and instabilities in the mesh. Increasing the density enabled faster processing times due to the time step of the explicit finite element code used being limited by the speed of the stress wave (dependent on the speed of sound through the material) moving through the structure. The material was assigned a coefficient of thermal expansion that could be adjusted via a scale factor to model the tensioning of the yarns. Once again the value chosen was optimised for model run time and stability. The material of the compaction plates were modelled as rigid.

SECTION PROPERTIES

The beams in each yarn bundle were represented as a Hughes-Liu beam section type that allowed the user to define the cross section of each beam exactly, thus allowing contact algorithms to work correctly.

BOUNDARY CONDITIONS

The ends of each yarn were allowed to translate in the through thickness direction and allowed to rotate in all three dimension. The rigid plates were fixed in rotation and in-plane translation directions, allowing only vertical movement.

THERMAL LOADING

A linear temperature drop was applied to the mesh in order to apply a tensile force on all the yarns. This had the effect of straightening the yarns that were not already fully straight i.e. the warp weavers and weft as well as causing the collapse of the bundle cross section into something approaching the lenticular section seen in the sectioned fabric samples (see

Figure ***4***). The straightening of the warp weavers and weft yarns caused a decrease in thickness of the fabric. Trials showed that a slow temperature drop over 10 seconds with a suitable CTE gave a stable change in thickness over a reasonable time. Once the thickness reached the measured as-woven thickness of a real fabric sample the temperature was held constant at that point until the termination of the solution.

COMPACTION

The rigid plates were then subject to a prescribed displacement regime that held them stationary until the end of the thermal loading cycle. The plates were then subjected to a high initial velocity to rapidly bring them close to the surface of the fabric and then the

plate velocity was lowered to a very gradual compaction of the fabric. The slow compaction speed was chosen to increase the stability of the beams under loading.

CONTACT MODELLING

The contact between yarns was controlled by the "Automatic General" contact option in the LS-Dyna software. The contact area excluded the extended parts of the yarns away from the area compacted by the plates to reduce analysis time. A yarn-to-yarn frictional coefficient of 0.5 was introduced. This value was arrived at by incremental testing of different coefficients and choosing the best one with respect to the generation of realistic yarn shapes and model stability.

Figure 4 Effect of thermal tensioning of weavers causing decrease in thickness of mesh .

OBSERVATIONS

Compacted samples of the modelled fabric were manufactured via resin transfer moulding (RTM) and subsequently sectioned and scanned using X-ray computed tomography (CT) which produced detailed images of the fabric internal structure. Further details of the experimental characterisation of the modelled fabric can be found in Mahadik et al. [21]. This allowed verification of the model output to be carried out by comparing the model geometry with that of the real manufactured samples.

Visualisation of the results produced by the model showed good correlation with the fabric structure before compression, with a lenticular yarn cross section being formed under thermal load. A good representation of the final compacted fabric internal

structure has been achieved. Distinctive architectural features such as local crimp and resin rich areas at weaver/weft crossover points and flattening of the weaver under compaction as seen in the CT scan were captured well by the model (see Figure 5 and Figure 6.)

Figure 5 Weft cross section of compacted sample and fabric model.

Figure 6 Warp weaver cross section of compacted sample and fabric model.

Observations of tow cross section shape showed that thinning and spreading of the yarns in the finite element model was greater than in the moulded sample, especially in the warp weavers. An illustration of this can be seen in Figure 7 where the cross section shape of the internal warp weaver yarns highlighted is significantly wider and thinner than that seen in a potted sample at the same volume fraction. This excess spreading can be attributed to the lack of any control of the beam bundle shape other than the coefficient of friction used for the entire model via the contact parameters. Additionally the approximation of yarn as a bundle of only nineteen beams rather than the many thousand of individual fibres present in a real yarn provides a reduced amount of yarn entanglement and frictional interaction that could mitigate excess tow spreading.

Figure 7 Comparison of yarn cross section shape in a weaver yarn in a) FE model and b) infused fabric sample

MODEL ANALYSIS AND VERIFICATION

A statistical analysis of out of plane yarn crimp in each yarn direction of the FE model was carried out. The local, out of plane yarn crimp of individual tows was measured by viewing a cross-section of the model and discretizing a single tow using a series of points plotted along its centre line (Figure). The absolute local angle between two adjacent points could then be calculated from their coordinates. Yarn crimp was defined as the local angle of deviation from a specified horizontal datum for each yarn.

The overall crimp in each yarn direction could then be calculated from the localized crimp data across several yarn planes and these average results broken down into a frequency distribution to highlight instances of higher crimp.

Figure 8 Method for calculating yarn crimp using tow discretization method [21]

The statistical analysis was extended to assess the size and shape of the distinctive resin rich regions left between layers of weaver yarns. These were caused by the path of the yarn leaving large gaps between yarn layers where resin rich regions subsequently developed. Resin pockets seen in the weft yarn planes were orthogonal cross sections of the channels in the warp direction. Figure shows a 3D representation of one of these channels and the images they produce when sectioned in the warp weaver and weft direction. The average dimensions of a single resin pocket were calculated from the yarn images by digitally separating the resin and yarn and outlining the resin rich regions.

A similar analysis was conducted on a series of resin transfer moulded angle interlock fabric samples manufactured to different thicknesses. Images in the three yarn planes were obtained using x-ray computed tomography and a series of post-process image enhancement techniques [21].

Figure 9 Schematic showing dimension definitions and CT scan views of the weaver resin channel

RESULTS: YARN CRIMP

Figure presents the mean yarn crimp data in the warp, weft and weaver yarns in both the modelled fabric and the equivalent laboratory-manufactured samples. The results for yarn crimp and resin channel size and shape for the laboratory manufactured samples are taken from work conducted by the author in a previous study [21] and are reproduced here for comparison and to validate the finite element model fabric architecture prediction. The correlation between the model prediction and the experimental results is very good, matching the trend across the volume fraction range within 1-1.5°. A comparison of the more detailed frequency distribution of local crimp data further illustrates the good agreement between the finite element model and the experimental data. Figure 7 shows a bar graph comparison of the frequency distribution of local crimp in the weft yarns throughout the volume fraction range and is typical of the accuracy achieved by the model prediction. A complete summary of the local crimp frequency distribution results is presented in tabular form (Tables 1-3). The only major discrepancy occurred in the warp yarns at 55%-60% volume fraction where the model

predicted a much higher proportion of the yarn to be crimped by more than 0-5° than the experimental data.

Figure 10 Mean yarn crimp directions in FE model and moulded fabrics

Figure 7. Frequency distribution of crimp in weft yarns at 50% VF

Table 1. Frequency distribution of crimp in warp yarns

Table 2. Frequency distribution of crimp in weft yarns

Table 3. Frequency distribution of crimp in warp weaver yarns

RESULTS: RESIN CHANNELS

Correlation between the FE model and the experimental data was good with respect to the overall resin channel volume, with the FE model predictions being within 10%.

However, detailed results for the individual tow cross sections showed much larger differences. Figure 8 shows the breakdown of the average dimensions of a single weaver resin channel. The trends of both the model and experimental data were similar but the absolute values did not correspond very closely except in the height dimension.

The FE model underestimated the length of the resin channel to a large degree, particularly at lower volume fractions between 50-55%. The model results also

overestimated the width of each resin channel by approximately 2mm throughout the compaction range.

These differences were attributed to the greater degree of tow spreading seen in the FE model than in the moulded fabrics. Each multi-element yarn had no user-controlled cohesive properties other than the applied contact friction between elements. This lead to greater spreading and deformation of the tow cross section compared to their manufactured counterparts that retained their shape more consistently under pressure perhaps due to fibre treatments, binder coatings or greater yarn filament entanglement.

Figure 8 Resin channel dimensions: FE model prediction and experimental results

CONCLUSION

A kinematic model of a 3D woven fabric with a layer-to-layer angle interlock structure using beam elements in the finite element software LS-Dyna, was created. This was based on multi-element digital chain technique developed by Miao and Zhou [18,19]. A tension load was applied to the fabric yarns via a thermal load in order to reduce the thickness to match that of the real fabric followed by compaction between two rigid plates to a thickness of a moulded fabric sample. Comparisons of general architectural features such as local high-crimp areas in yarns and resin pockets with manufactured fabric samples showed a good representation of a real compacted fabric. Detailed statistical analyses of out-of-plane yarn crimp and resin channel dimensions was carried out on both the finite element model and RTM manufactured samples at different levels of compaction. Correlation between the model and the manufactured samples was very

good with respect to yarn crimp in all yarn directions. Analysis of resin channel dimensions showed greater discrepancies that were attributed to a lack of yarn cohesive forces in the modelled digital-element yarns. This indicated that further development of the model should include some form of control of yarn cross section deformation.

REFERENCES

[1] Tan P, Tong L, and Steven G.P. Modelling for predicting the mechanical properties of textile composites – A review. Composites Part A 1997; 28A: 903-922

[2] Lomov SV, Huysmans G, Luo Y, Parnas RS, Prodromou A, Verpoest I, Phelan FR. Textile composites: modelling strategies. Composites Part A 2001; 32: 1379-1394

[3] Lomov SV, Ivanov DS, Verpoest I, Masaru Z, Kurashiki T, Nakai H, Hirosawa S. Meso-FE modelling of textile composites: Road map, data flow and algorithms. Composites Science and Technology 2007; 67: 1870-1891

[4] Bogdanvich A. Multi-scale modelling, stress and failure analyses of 3D-woven composites. J Mater Sci 2006; 41: 6547-6590

[5] Wang XF, Wang XW, Zhou GM, Zhou CW. Multi-scale analyses of 3D woven composite based on periodicity boundary, Journal of Composite Materials 2007; 41: 1773-1788

[6] Tan P, Tong L, Steven GP. Behaviour of 3D orthogonal woven CFRP composites. Part II. FEA and analytical modelling approaches. Composites: Part A 2000; 31: 273-281

[7] Lomov SV, Ivanov DS, Perie G, Verpoest I, Modelling 3D fabrics and 3D-reinforced composites: challenges and solutions. 1st World Conference on 3D Fabrics, Manchester. 9-11-04-2008.

[8] Chen B, Chou Tsu-Wei, Compaction of woven-fabric preforms in liquid composite moulding processes: single-layer deformation. Composites Science and Technology 1999; 59:1519-1526

[9] Lomov SV, Verpoest I. Compression of woven reinforcements: a mathematical model. Journal of Reinforced Plastics and Composites 2000. 19: 1329-1350

[10] Potluri P, Parlak I, Ramgulam R, Sagar TV. Analysis of tow deformations in textile performs subjected to forming forces. Composites Science and Technology 2006; 66: 297-305

[11] Chen ZR , Lin Y, Kruckenberg T. A micromechanical compaction model for woven fabric preforms. Part I: Single layer. Composites Science and Technology 2006; 66: 3254-3262

[12] Chen ZR, Ye L. A micromechanical compaction model for woven fabric preforms. Part II: Multilayer. Composites Science and Technology 2006; 66: 3262-3272

[13] Potluri P, Sagar TV. Compaction modelling of textile preforms for composite structures. Composite Structures 2008; 86: 177-185

[14] Lin H, Sherburn M, Crookston J, Long A, Clifford MJ, Jones IA. Finite element modelling of fabric compression. Modelling and Simulation in Materials Science and Engineering 2008; 16:1-16

[15] Potluri P, Long A, Young RJ, Lin H, Shyng YT, Manan A. Compliance modelling of 3D weaves. Presented at 16th International Conference on Composite Materials, Kyoto, Japan 2007.

[16] Wang Y, Sun X. Digital-element simulation of textile processes. Composites Science and Technology 2001. 61: 311-319

[17] Durville D. Numerical simulation of entangled materials mechanical properties. Journal of Material Science 2005; 40: 5941-5948

[18] Miao Y, Zhou E, Wang Y, Cheeseman BA. Mechanics of textile composites: Micro-geometry. Composites Science and Technology 2008; 68:1671-1678

[19] Zhou G, Sun X, Wang Y. Multi-chain digital element analysis in textile mechanics. Composites Science and Technology 2004; 64: 239-244

[20] Zhou E, Mollehauer D, Iarve E. A realistic 3-D textile geometry model. Presented at 17th International Conference on Composite Materials, Edinburgh, UK 2009.

[21] Mahadik Y, Hallett S, Robson-Brown K. Characterisation of 3D woven composite internal architecture and effect of compaction. Composites: Part A (2010), doi:10.1016/j.compositesa.2010.02.019

FIGURES

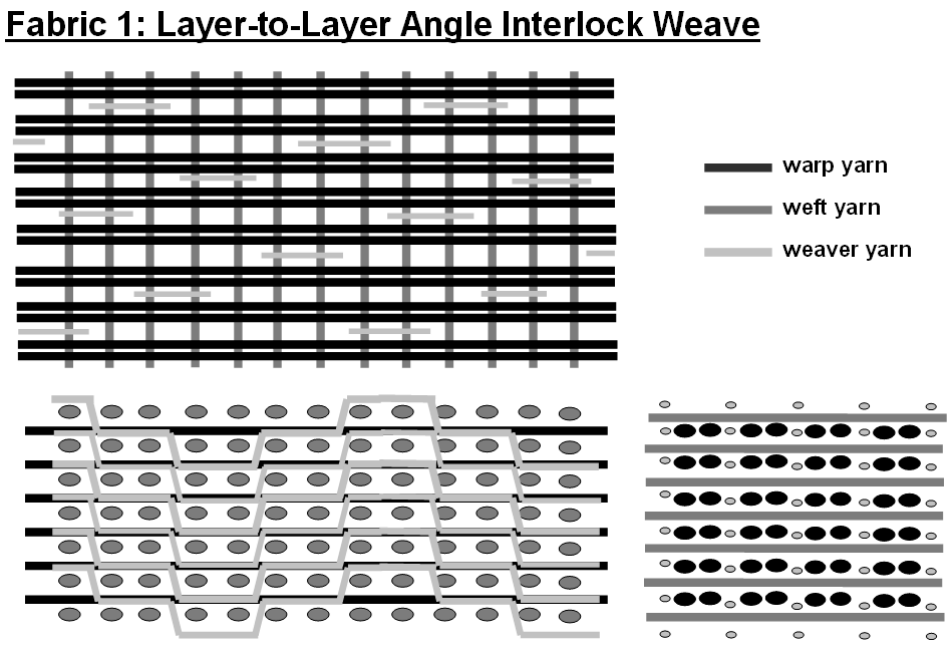

Figure 9 Schematic of layer-to-layer angle interlock fabric.

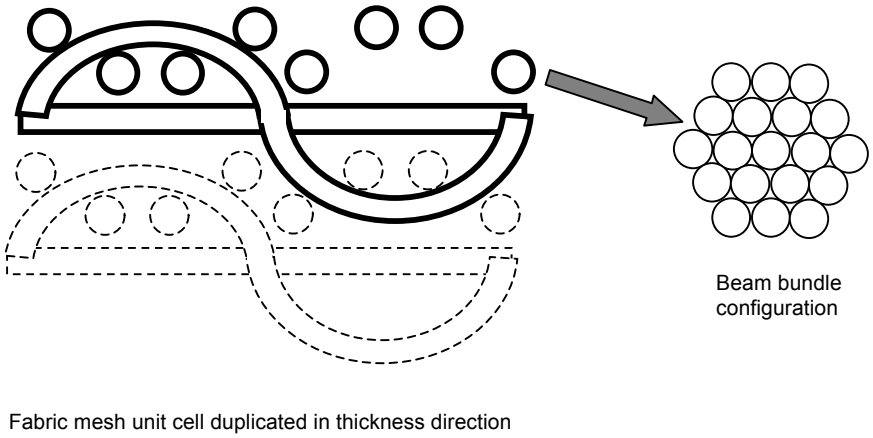

Figure 10 Schematic of finite element mesh unit cell and tow beam bundle configuration.

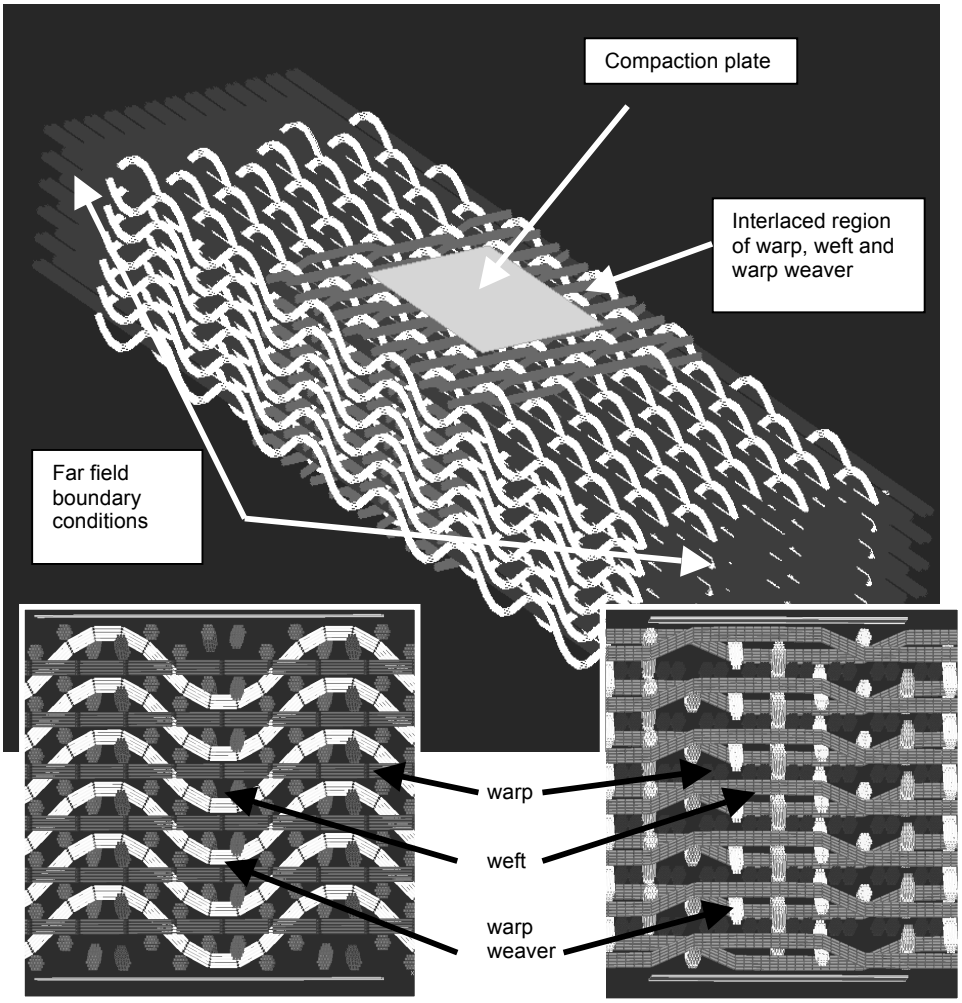

Figure 11 Final finite element mesh with sections through interlaced region inset.

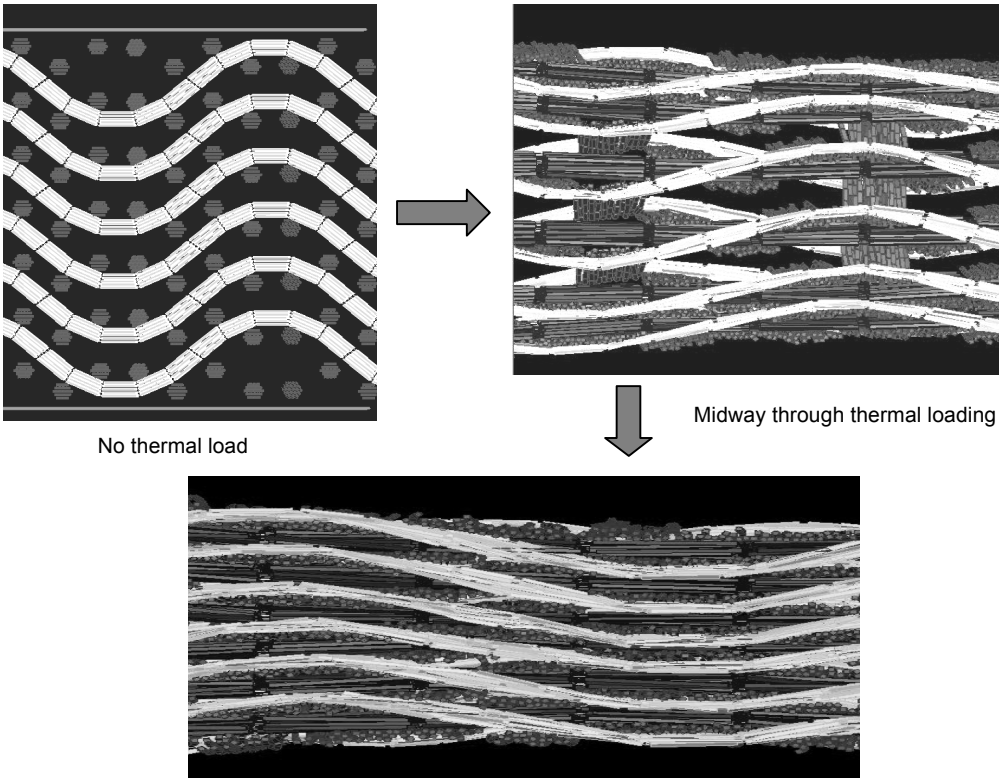

Figure 12 Effect of thermal tensioning of weavers causing decrease in thickness of mesh

.

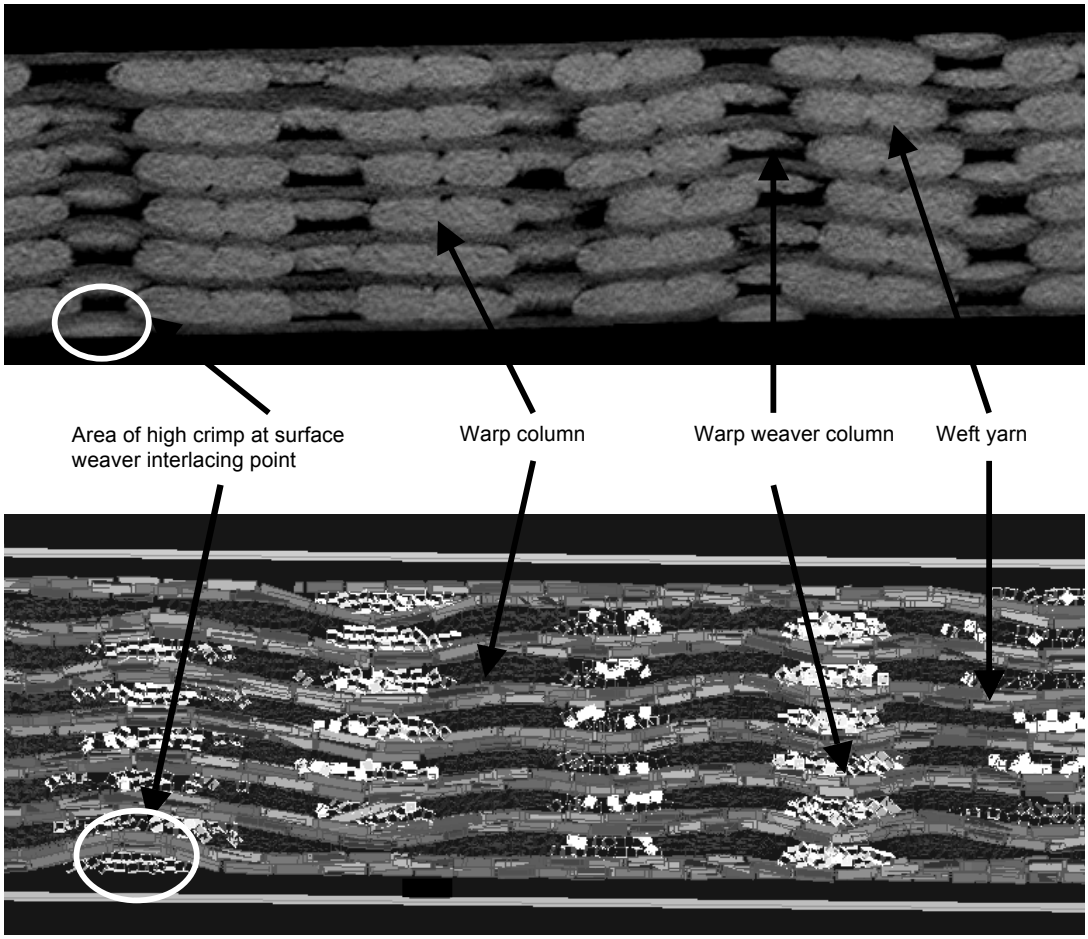

Figure 13 Weft cross section of compacted sample and fabric model.

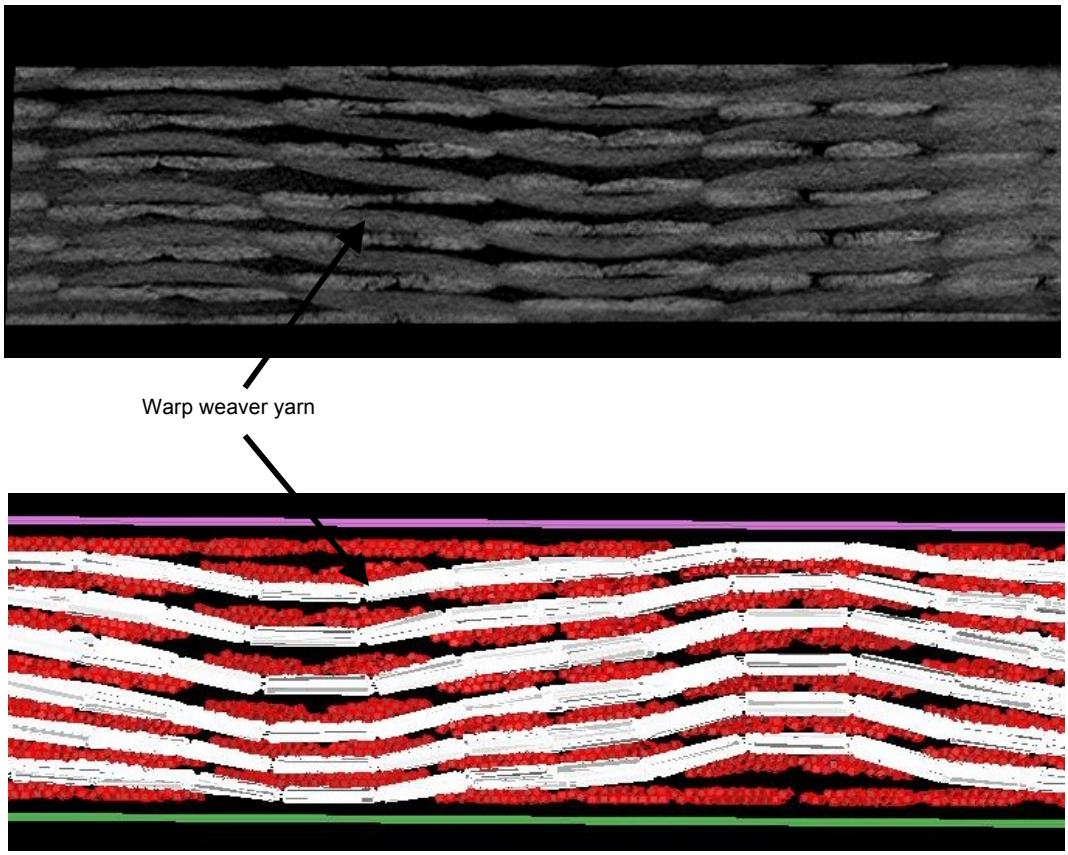

Figure 14 Warp weaver cross section of compacted sample and fabric model.

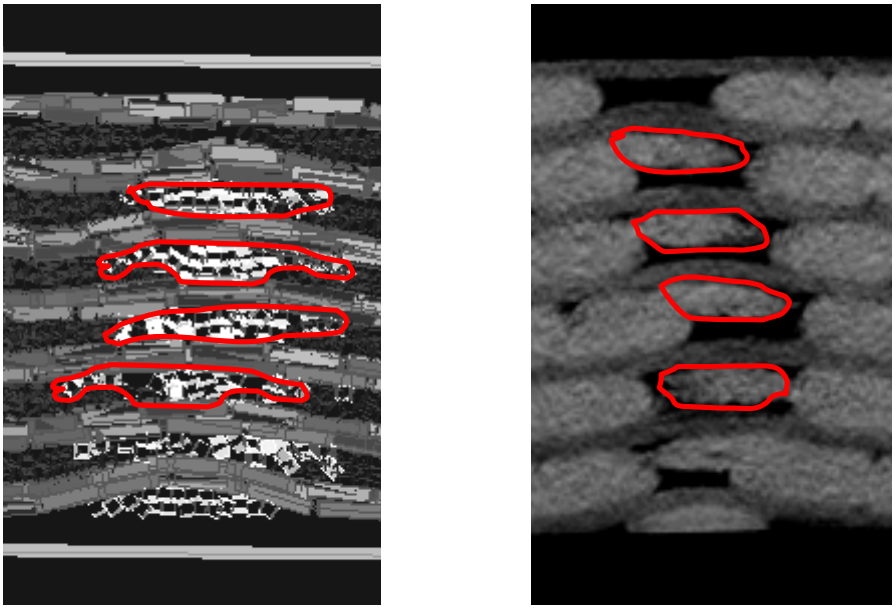

a) b)

Figure 7 Comparison of yarn cross section shape in a weaver yarn in a) FE model and b) infused fabric sample

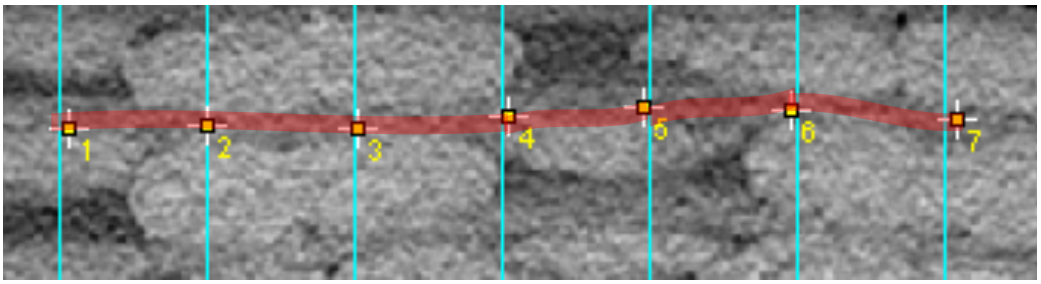

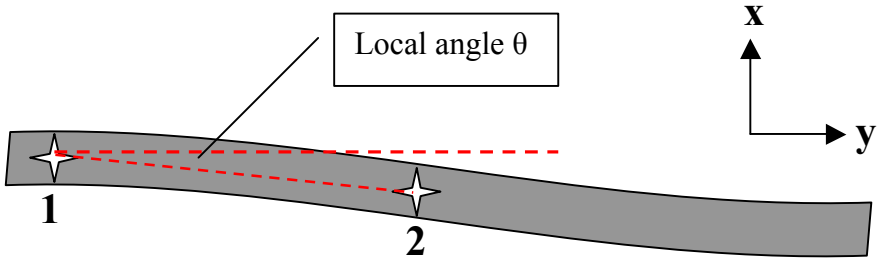

$$\theta = \text{Tan}^{-1}\left(\frac{y_1 - y_2}{x_1 - x_2}\right)$$

Figure 8 Method for calculating yarn crimp using tow discretization method [19]

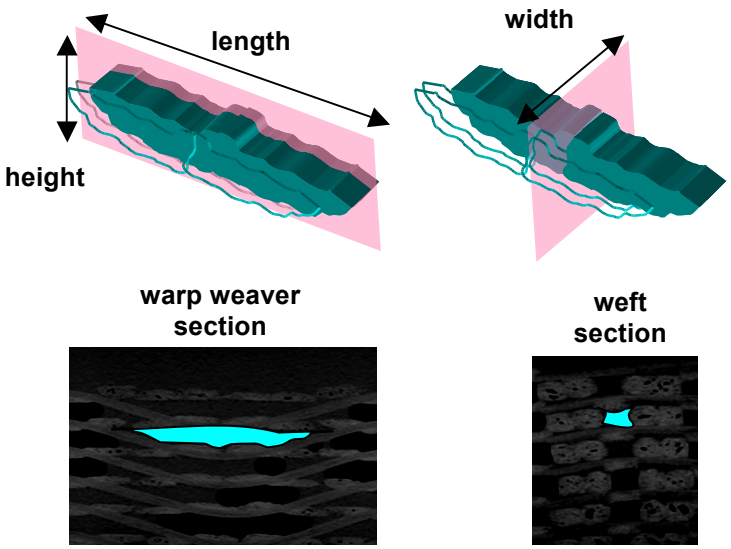

Figure 9 Schematic showing dimension definitions and CT scan views of the weaver resin channel

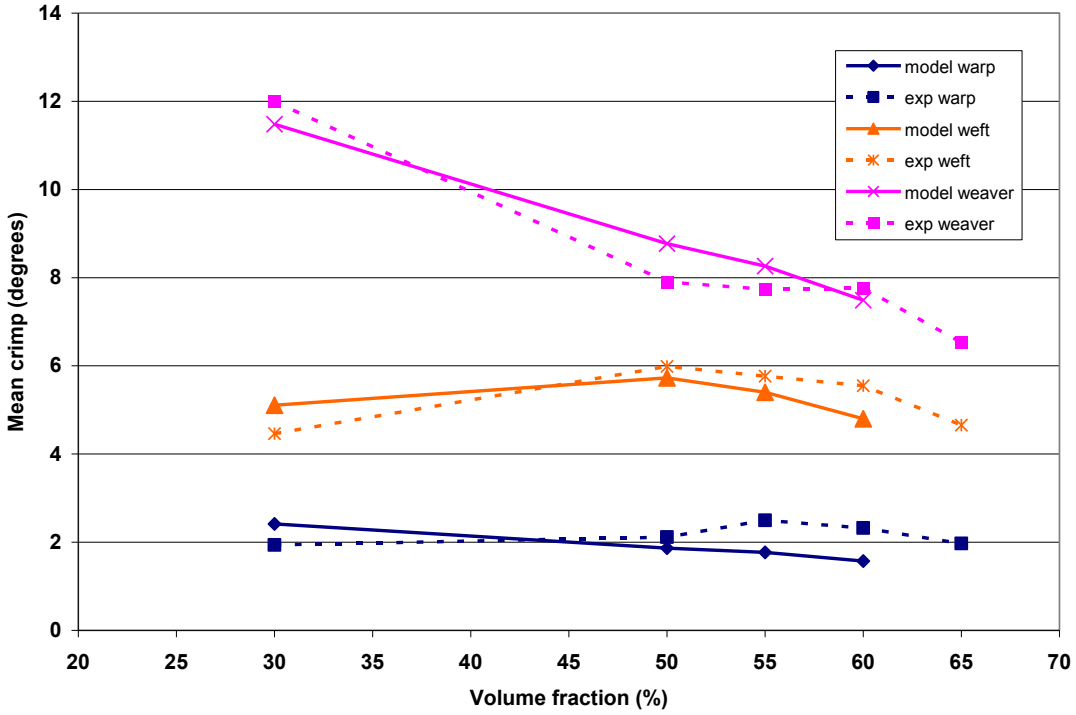

Figure 10 Mean yarn crimp directions in FE model and moulded fabrics

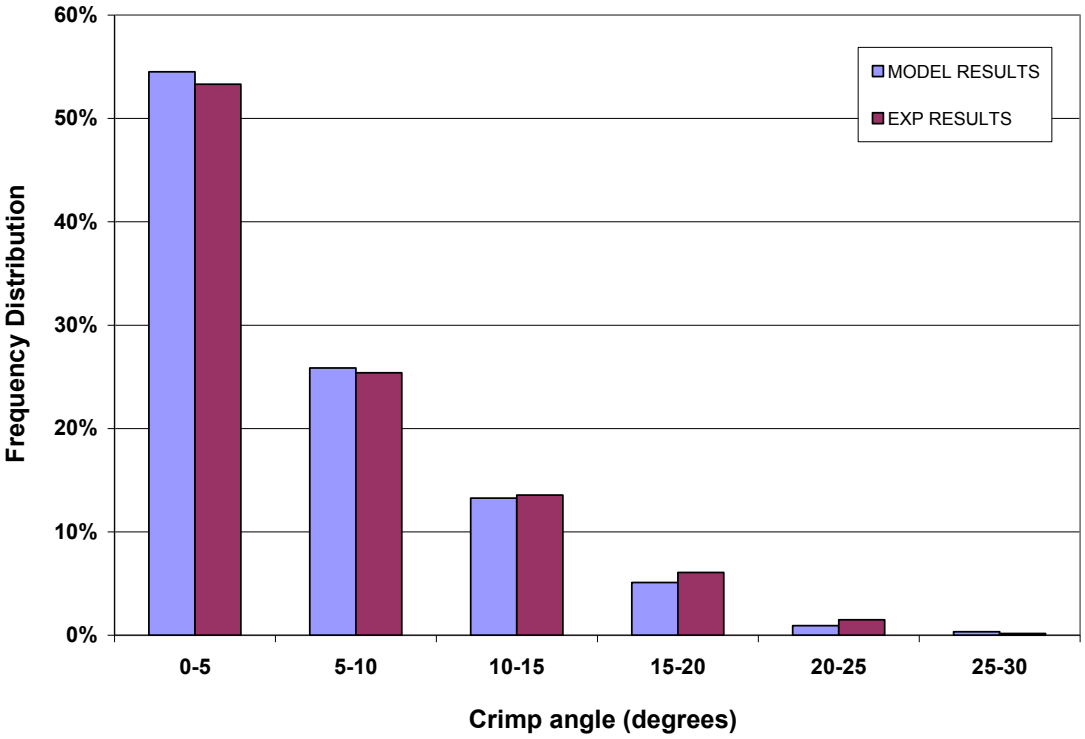

Figure 15. Frequency distribution of crimp in weft yarns at 50% VF

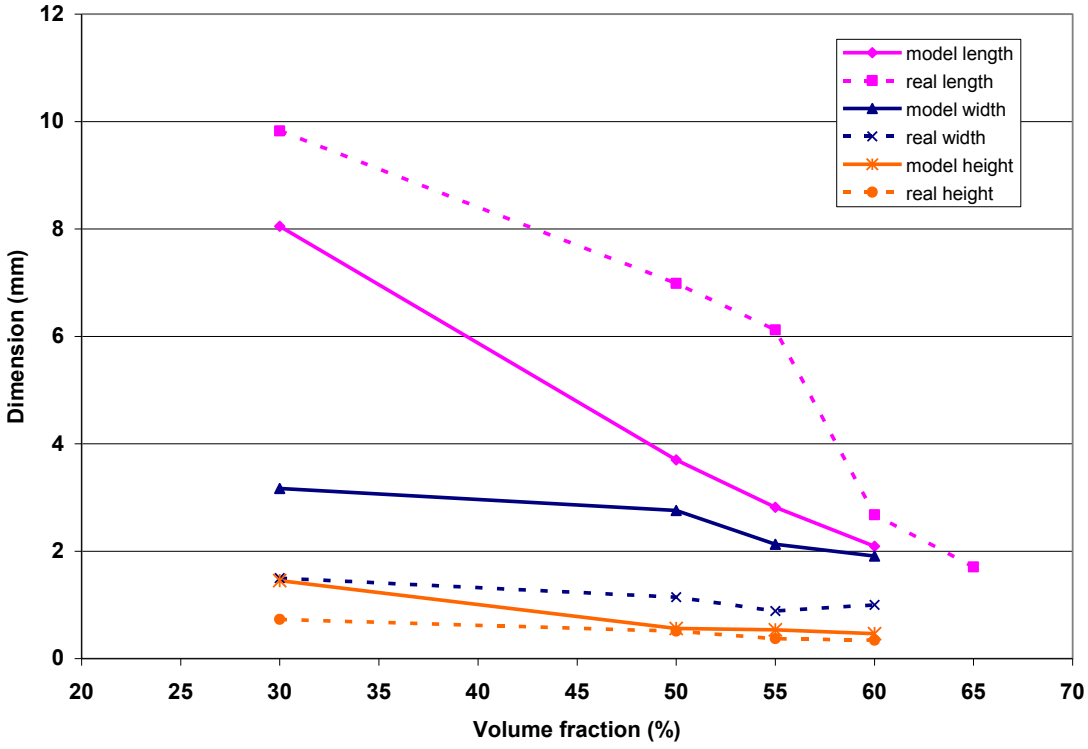

Figure 16 Resin channel dimensions: FE model prediction and experimental results

TABLES

Table 1. Frequency distribution of crimp in warp yarns

VF		Crimp (degrees) 0-5	5-10	10-15	15-20	20-25	25-30
30%	MODEL	86.1%	12.4%	1.2%	0.0%	0.3%	0.0%
	EXP	98.0%	2.0%	0.0%	0.0%	0.0%	0.0%
	DIFFERENCE	**11.8%**	**10.3%**	**1.2%**			
50%	MODEL	92.6%	7.1%	0.2%	0.1%	0.0%	0.0%
	EXP	91.9%	8.0%	0.1%	0.0%	0.0%	0.0%
	DIFFERENCE	**0.7%**	**0.9%**	**0.1%**			
55%	MODEL	94.0%	5.9%	0.1%	0.0%	0.0%	0.0%
	EXP	86.8%	12.5%	0.7%	0.0%	0.0%	0.0%
	DIFFERENCE	**7.1%**	**6.6%**	**0.5%**			
60%	MODEL	61.8%	25.5%	10.1%	2.0%	0.6%	0.0%
	EXP	88.8%	11.0%	0.2%	0.0%	0.0%	0.0%
	DIFFERENCE	**26.9%**	**14.5%**	**9.9%**	**2.0%**	0.6%	

Table 2. Frequency distribution of crimp in weft yarns

VF		Crimp (degrees) 0-5	5-10	10-15	15-20	20-25	25-30
30%	MODEL	60.6%	23.2%	11.4%	3.5%	1.1%	0.2%
	EXP	65.5%	27.4%	6.3%	0.7%	0.0%	0.0%
	DIFFERENCE	**4.8%**	**4.2%**	**5.0%**	**2.8%**	**1.1%**	**0.2%**
50%	MODEL	54.5%	25.9%	13.3%	5.1%	0.9%	0.3%
	EXP	53.3%	25.4%	13.6%	6.1%	1.5%	0.2%
	DIFFERENCE	**1.2%**	**0.5%**	**0.3%**	**1.0%**	**0.6%**	**0.2%**
55%	MODEL	54.5%	27.6%	14.4%	3.0%	0.4%	0.1%
	EXP	54.4%	25.8%	13.1%	5.3%	1.1%	0.2%
	DIFFERENCE	**0.1%**	**1.8%**	**1.4%**	**2.4%**	**0.7%**	**0.2%**
60%	MODEL	61.8%	25.5%	10.1%	2.0%	3.0%	0.3%
	EXP	59.5%	22.7%	9.9%	5.4%	2.4%	0.2%
	DIFFERENCE	**2.3%**	**2.9%**	**0.2%**	**3.5%**	**0.6%**	**0.1%**

Table 3. Frequency distribution of crimp in warp weaver yarns

VF	CRIMP (degrees)	0-5	5-10	10-15	15-20	20-25	25-30
30%	MODEL	17.3%	20.4%	32.6%	23.6%	5.4%	0.7%
	EXP	19.8%	19.5%	26.7%	32.5%	1.6%	0.0%
	DIFFERENCE	**2.6%**	**0.9%**	**5.9%**	**8.9%**	**3.8%**	**0.7%**
50%	MODEL	29.1%	29.7%	26.1%	12.5%	2.3%	0.3%
	EXP	33.1%	33.3%	23.0%	9.0%	2.6%	0.3%
	DIFFERENCE	**4.0%**	**3.6%**	**3.1%**	**3.5%**	**0.3%**	**0.0%**
55%	MODEL	34.8%	26.3%	24.8%	12.1%	1.8%	0.3%
	EXP	38.3%	28.1%	23.1%	7.5%	3.6%	0.7%
	DIFFERENCE	**3.6%**	**1.9%**	**1.7%**	**4.6%**	**1.8%**	**0.5%**
60%	MODEL	43.0%	24.9%	18.8%	9.8%	3.1%	0.3%
	EXP	41.8%	26.4%	17.5%	10.0%	1.6%	1.1%
	DIFFERENCE	**1.2%**	**1.4%**	**1.3%**	**0.2%**	**1.5%**	**0.8%**